

# Delocalization in two and three-dimensional Rydberg gases

G. Abumwis, Matthew T. Eiles, Alexander Eisfeld\*

Max-Planck-Institut für Physik komplexer Systeme, Nöthnitzer Str. 38, D-01187 Dresden, Germany

E-mail: eisfeld@mpg.pks.de\*

**Abstract.** We calculate the eigenstates of an interacting Rydberg gas and use a coherence measure to quantify and analyze their delocalization throughout the random gas. This study reveals that the dipole-dipole interactions lead to remarkably delocalized wave functions, which we examine in further detail by varying the dimension of the gas, the anisotropy of the interaction, and the power law exponent of the interaction. We find that the delocalized states are robust against various types of perturbations.

## 1. Introduction

Resonant dipolar interactions are ubiquitous in nature. They are the subject of extensive study in molecular aggregates [1] and photosynthetic systems [2]. These systems are typically rather regularly arranged and exhibit excitonic states that are delocalized over several particles. Such regular arrangements have also been extensively studied in other systems, for example in ultracold molecules [3] or Rydberg atoms [4]. A renewed interest in *random* arrangements has developed in recent years, stemming from measurements on very dilute gases containing both ground state atoms and atoms in their first excited state [5–9]. The extent to which these states are delocalized is debated [10, 11].

An ultracold gas of Rydberg atoms is an ideal scenario to study strongly-interacting coherent systems [12–15]. The long-range nature of Rydberg interactions and the sufficiently long atomic lifetimes allow coherent processes to take place on experimental timescales without any significant decoherence due to thermal motion or spontaneous decay [16–20]. Although it has recently become possible to prepare the Rydberg atoms in well-defined positions using an optical lattice or a tweezer array, atoms are typically probabilistically arranged in a cloud. In conjunction with the freezing out of their motional degrees of freedom, this creates an unusual situation whereby a strongly-interacting random system with long coherence times can be readily studied and controlled in the laboratory.

Since the key properties of Rydberg atoms scale with the level of excitation and can thereby be tuned extensively, experimentalists can access a wide parameter range [21–23].

The interaction between two well-separated Rydberg atoms is determined by the multipole expansion of each Rydberg charge cloud [18]. If both atoms are in the same quantum state, the interaction is typically second-order in the dipole-dipole term,  $V_6 \propto \frac{\nu^{11}}{R^6}$ , where  $R$  is the interparticle separation and  $\nu$  is the principal quantum number [24] ‡. In the absence of external fields to polarize the atomic states, this interaction is essentially isotropic. When the two atoms are in different states connected by a non-zero dipole transition matrix element. Now, the dominant interaction is the resonant dipole-dipole interaction,  $V_3 \propto \frac{\nu^4}{R^3}$ . Unlike before, this interaction is strongly anisotropic, depending on the relative orientation of the interparticle distance with the quantization axis, and hence dependent on the  $m_l$  quantum number as well [26].

Due to the large interatomic separations at typical densities, these interactions are usually small compared to the energy separation between states with different principal quantum number. This implies that an essential state picture can typically be adopted. In our case, the Hilbert space of each atom is restricted to only include two Rydberg states coupled by the dipole matrix element. For concreteness, we consider the  $s$  and  $p$  Rydberg states with the same  $\nu$ . We label these states  $|\uparrow\rangle$  and  $|\downarrow\rangle$ , respectively. This two-state approximation is adequate for most parameter regimes, but it can be invalidated in special circumstances, such as at very high density or principal quantum number, in the presence of significant external fields, or if unfavorable parameters are chosen, leading to accidental near-degeneracies with states outside of our two-state subspace [27].

We consider the simplest scenario of an interacting Rydberg gas: the single-exciton case, where one  $|\uparrow\rangle$  exciton is added to an assembly of  $N - 1$  Rydberg atoms all in the state  $|\downarrow\rangle$ . In the absence of interactions, the single-exciton wave functions are of the form

$$|n\rangle = |\downarrow\rangle_1 \cdots |\uparrow\rangle_n \cdots |\downarrow\rangle, \quad (1)$$

where the atom at position  $n$  is promoted to the  $\uparrow$  state. Interactions cause this excitation to be shared coherently between sites, as described by the collective eigenstate

$$|\psi_\ell\rangle = \sum_n c_n^{(\ell)} |n\rangle. \quad (2)$$

‡ A notable exception is the case of a so-called “Förster resonance” [25], occurring when the considered pair state is nearly resonant with another pair state.

Recently, we studied the eigenstates of a three-dimensional random gas of  $N$  Rydberg atoms and focused in particular on their delocalization as described by the distribution of coefficients  $c_n^{(\ell)}$  [28]. We observed that the majority of these collective states are remarkably delocalized, having coherences – a measure of delocalization – growing linearly with the number of gas particles. This delocalization in spite of the random arrangement of particles is facilitated by the dipole-dipole interactions. The random spatial arrangement of the atoms lead to nearby clusters of two or more atoms. These interact strongly due to their proximity and energetically decouple from the remaining system, which now has no clusters and resembles a network with quasi-homogeneous spacing. Because of the long-range nature of the dipole-dipole interaction the atoms remaining in this network have non-negligible interactions even at these larger separations, and can therefore delocalize over many sites.

While Ref. [28] focuses on the experimentally most relevant scenario of dipole-dipole interactions in a *three-dimensional* (3D) gas, in the present work we additionally study two-dimensional (2D) arrangements. A two-dimensional gas can be realized in present-day Rydberg experiments with sufficiently tight confinement [29], and provides a very useful experimental complement to the three-dimensional gas as it allows one to modify the isotropy of the interaction in a simple way by varying the relative angle between an applied magnetic field and the confinement axis. The 2D case also relates to the investigation of molecules randomly placed on surfaces [30,31]. Much additional information about the nature of the delocalized states observed in Ref. [28] can be gleaned from the study of other power-law interactions, system dimensions, and interaction isotropy, as we undertake in the present work. We also study the dependence of the localization on the structure of the interaction Hamiltonian, which can be modified due to disorder or the Rydberg blockade, effects which can either reduce or increase the degree of localization. Through these various manipulations of the system Hamiltonian we can build a body of observations which can reveal trends and dependencies of the localization in the Rydberg gas and embed our conclusions in the broader context of strongly interacting finite systems.

## 2. Theoretical background

### 2.1. Long-range interactions in the essential state Hamiltonian

We consider the single-exciton sector of the full many-body Hamiltonian of the interacting Rydberg gas, which is spanned by the states  $|n\rangle$ . In this basis, the

single-exciton Hamiltonian takes the form

$$H = \sum_{n=1}^N \epsilon_n |n\rangle\langle n| + \sum_n \sum_{m \neq n} V_{nm}(\vec{R}_n, \vec{R}_m) |n\rangle\langle m|. \quad (3)$$

The on-site energies  $\epsilon_n$  are constant for each atom, but later on we will introduce diagonal disorder to probe the robustness of the delocalized states. The generic form of the interaction is that of a power-law,

$$V_{nm}(\vec{R}_n, \vec{R}_m) = \frac{1}{3} \frac{\mu^2}{|\vec{R}_n - \vec{R}_m|^\alpha} f(\theta_{nm}), \quad (4)$$

where  $\mu$  is the transition dipole between  $\uparrow$  and  $\downarrow$  states. In general, the presence of degenerate magnetic sublevels in the  $\downarrow$  and  $\uparrow$  states result in this operator taking on a tensorial form [27,32]; to simplify it we have assumed that a magnetic field of a few tens of Gauss is applied to the gas. This field strength is not strong enough to modify the Rydberg states themselves, but shifts each  $m_l$  level at a rate of 1.4MHz/G via the Zeeman term [4]. In this fashion, one can excite only the  $m_l = 0$  states and thus simplify the angular dependence of the interaction to a function  $f(\theta_{nm})/3$ , depending only on the relative angle between the interparticle distance and the magnetic field. The factor  $\frac{1}{3}$  comes also from this separation of degenerate  $m$ -sublevels. For the 3D Rydberg gas studied in Ref. [28],  $\alpha = 3$  and the interaction is anisotropic:  $f(\theta_{nm}) = (1 - 3 \cos^2 \theta_{nm})$ . In the present work we study also isotropic interactions, having  $f(\theta_{nm}) = 1$ , as can be implemented experimentally in the two-dimensional gas by orienting the magnetic field perpendicular to the plane of atoms.

### 2.2. Absorption spectrum

For a given random realization of atomic positions,  $H$  is diagonalized to obtain the eigenstates. The transition frequencies between  $s$  and  $p$  states range from a few GHz down to hundreds of MHz. Therefore, the eigenstates can be excited from the initial state,  $|G\rangle = |\downarrow\rangle_1 \dots |\downarrow\rangle_N$ , by microwave absorption. A specific state  $|\psi_\ell\rangle$  can be excited provided that this microwave frequency is detuned from the atomic transition by that state's eigenenergy and that the transition strength,  $\mathcal{A}_\ell$ , is finite. For a microwave where the electric field component is aligned parallel to the external magnetic field, the transition strength is

$$\mathcal{A}_\ell = \left| \langle \psi_\ell | \sum_n c_n^{(\ell)} |G\rangle \right|^2 = \left| \sum_n c_n^{(\ell)} \right|^2. \quad (5)$$

This assumes identical transition dipoles and weak interactions with the microwave. The presence of large absorption strengths requires a large delocalization:

a delocalization of  $N$  can only be achieved by a perfectly delocalized collection of atoms, i.e.  $c_{n\ell} = N^{-1/2}$ . However, the reverse is not true: a large delocalization does not imply a large absorption, and hence the absorption spectrum is not a sensitive probe of delocalized states.

### 2.3. Localization measures

The delocalization of a quantum state can be quantified using a variety of measures. The two most common ones, due to their ease of interpretation and accuracy at describing the relevant quantities of the wave functions, are the coherence and the participation ratio. Using the density matrix,  $\rho_{nm}^{(\ell)} = |\psi_n^{(\ell)}\rangle\langle\psi_m^{(\ell)}|$ , the coherence is defined as [33]

$$C_\ell = \sum_n \sum_{m \neq n} |\rho_{nm}^{(\ell)}|. \quad (6)$$

Using only the wave function itself, the ‘‘participation ratio’’, sometimes called the inverse of the ‘‘inverse participation ratio’’ (IPR), is defined using

$$N_\ell^{\text{IPR}} = \left[ \sum_n \left( \rho_{nn}^{(\ell)} \right)^2 \right]^{-1}, \quad (7)$$

In general, the value of either measure corresponds roughly to the number of atoms coherently sharing the excitation. The IPR for a perfectly delocalized state having equal amplitude on each atom equals  $N$ , while the coherence is  $N - 1$ . A dimer state, with only two atoms participating, has a coherence of 1 and an IPR of 2. We show in the appendix that both coherence and IPR measures give similar results, but the coherence highlights asymmetries in the distributions and spectra that are less clear in the IPR.

### 2.4. Numerical implementation of the Rydberg gas

The positions of the Rydberg atoms are determined by the random positions of the ground state atoms and on the details of the excitation process. Typically, only a fraction ( $\sim 1\%$ ) of the ground state atoms are selected at random to become Rydberg atoms [21]. By varying the laser power, higher or lower densities can be achieved.

However, during this process the so-called Rydberg blockade mechanism can influence the spatial distribution of Rydberg atoms [34–37]. Due to the van der Waals  $V_6$ , the interaction energy of two adjacent Rydberg atoms in the  $\downarrow$  state can exceed the laser bandwidth and thus prevent their mutual excitation. The relevant length scale is given by the blockade radius  $R_B$ , which scales as  $R_B \propto (\nu^{11}/\Omega_{\text{Laser}})^{1/6}$ . Thus, for a given density of ground state atoms, both the principle

quantum number  $\nu$  and the laser bandwidth  $\Omega_{\text{Laser}}$  can be used to prevent the excitation of closely-spaced Rydberg atoms. This both reduces the density of  $\downarrow$ -state atoms relative to the initial ground-state gas density and also removes pronounced inhomogeneities in the gas formed by random clustering §. In the present work we use a simplified description of the blockade mechanism and assume that, when two or more ground state atoms are closer than  $R_B$ , only one of them can be excited into a Rydberg state and the others play no role. This is implemented in our simulation by removing from the initially seeded atoms one from every pair which have a separation smaller than  $R_B$ . We therefore neglect the many-body nature of the blockaded state.

In our simulation, the positions of Rydberg atoms are drawn at random from a uniform distribution. We work in a parameter regime where motion induced by the dipole-dipole interaction can be neglected on the time scales of interest. Note that strong forces can be present between atoms in close proximity, leading to acceleration and a breakdown of the frozen gas approximation [41–45]. For extended atomic networks, conical intersections might play a role [46]. To take into account fluctuations due to the random gas realizations, we average over 2000 total iterations for each calculation. We take as the system volume a rectangle of volume  $L^D$ , where  $D = 2, 3$  is the dimension and  $L$  is the side length. For all cases we fix the number of atoms to  $N = 1000$ ; we can extrapolate to other  $N$  values using the scaling relations deduced in Ref. [28]. We note that any edge effects from the boundary of the simulation volume can be mitigated by choosing the largest possible value of  $N$  allowed by numerical capabilities. However, for the atomic densities, excitation efficiencies, and dimensions of a typical ultracold gas experiment, the number of Rydberg atoms produced per shot is typically on the order of 1000. As a result, these edge effects crudely model the physical boundaries of the laboratory gas. For certain trapping configurations the distribution of Rydberg atoms can have sharp boundaries within a specifically shaped area [29]; on the other hand, in atomic vapours the boundaries can be very diffuse. We have verified that the boundary effects are only minor by reproducing these results with a spherical distribution of atoms.

The Rydberg density  $n_{\text{Ryd}}$  is determined by the dimensions of the simulation volume following  $n_{\text{Ryd}} = N/(2R)^D$ . We define a set of scaled length and energy units which remove the dependence of the Hamiltonian on density and let us deal with dimensionless quantities only. We use the Wigner-Seitz radius,  $a_{\text{ref}}(D)$ , as

§ One can even use this blockade mechanism in conjunction with appropriate laser detuning to form anti-blockaded atoms in regular arrangements [38–40]

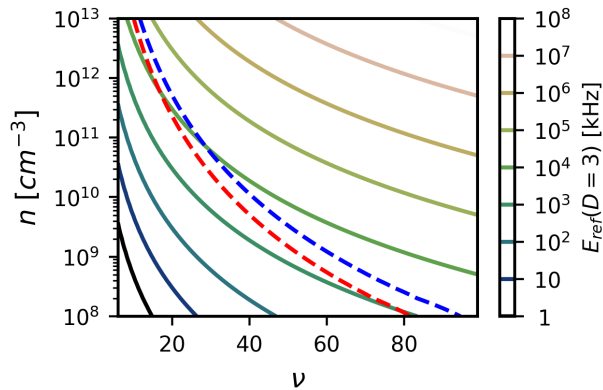


**Figure 1.** The available parameter space for a three-dimensional Rydberg gas of  $^{87}\text{Rb}$  atoms. Contours of constant  $E_{\text{ref}}(3)$  (Eq. 9) are shown as a function of principal quantum number  $\nu$  and Rydberg density  $n$ . The dashed contours give the parameter range required to achieve a blockade radius  $R_B = 0.5$ , in units of  $a_{\text{ref}}(3)$ , for two different values of  $\Omega_{\text{Laser}}$ , 0.1 MHz (red) and 0.5 MHz (blue).

our unit of length. This is defined in two and three dimensions as

$$a_{\text{ref}}(2) = \left( \frac{1}{\pi n_{\text{Ryd}}} \right)^{1/2}; \quad a_{\text{ref}}(3) = \left( \frac{3}{4\pi n_{\text{Ryd}}} \right)^{1/3}. \quad (8)$$

This unit of length, in turn, defines a characteristic energy scale. The nearest neighbour interaction energy (neglecting the anisotropy of the interaction) between two particles separated by the respective Wigner-Seitz radius is

$$E_{\text{ref}}(D) = \frac{1}{3} \frac{\mu^2}{[a_{\text{ref}}(D)]^\alpha}. \quad (9)$$

We measure energies in units of  $E_{\text{ref}}(D)$ . The density, principal quantum number  $\nu$ , and  $E_{\text{ref}}(D)$  are all related and can be tuned accordingly to match laboratory constraints, as shown for the case  $D = \alpha = 3$  in Fig. 1. For the transition dipole we use  $\mu = \mu_0 \nu^2$ , where  $\mu_0$  is the transition dipole between the ground and first excited state.

### 3. Results

Fig. 2 displays the distribution of coherences and eigenvalues of a random Rydberg gas interacting via the dipole-dipole interaction ( $\alpha = 3$ ). We present the results from the four possible combinations of anisotropic and isotropic interactions within two- and three-dimensional gases together in order to facilitate a phenomenological comparison. The distribution in the top left panel, for the three-dimensional gas with anisotropic interactions, is the main result of Ref. [28]. This distribution is narrower on the negative energy side than on the positive, and has a pronounced

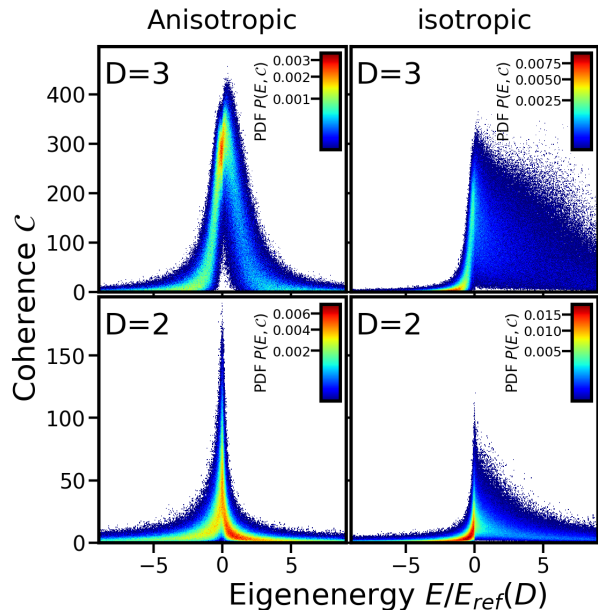


**Figure 2.** Coherence and energy distributions for the  $\alpha = 3$  interaction. The coherence binwidth is 0.5 and the energy binwidth is 0.01. The energy unit is  $E_{\text{ref}}(D)$ .

peak feature at very small negative energies but large coherences. For both positive and negative energies near zero almost all states have a large coherence, and essentially none have a low coherence value. In total, states with coherence values of nearly  $N/3$  are remarkably common, and localized states with coherence  $< 10$  are present only in the tails of this distribution. The large energy shifts of these states identify them as small clusters with strong interactions. Although the distribution is asymmetric in several important ways, the marginal coherence distributions integrated over either all negative or all positive energies are very similar, both resembling the overall marginal distribution plotted as the blue curve in the top left of Fig. 3. This distribution has been discussed in detail in Ref. [28]; it consists of two contributions. The first, highlighted in the inset, is composed of the tightly clustered states with very large interaction strengths. The second is the broad-tailed distribution of delocalized states which span roughly  $1/3$  of the gas.

As demonstrated by the top right panel of Fig. 2, this distribution is very sensitive to the anisotropy of the interaction. When the interaction is isotropic the overall delocalization decreases, and the asymmetry about zero energy becomes much stronger. At all negative energies except very close to zero, the states are all highly localized; in contrast, one can find highly delocalized states at all positive energies within the range considered here. Unlike in the anisotropic case, these blue-detuned states are spread almost

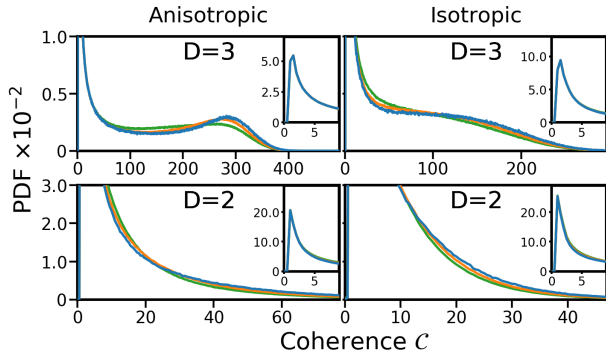


**Figure 3.** Coherence distributions for the  $\alpha = 3$  interaction and four different disorder strengths  $V$ : 0 (blue), 0.5 (orange), 1.0 (green), all in units of  $E_{\text{ref}}(D)$ . The coherence binwidth is 0.5. The insets show a closeup of the small coherence region.

uniformly over a large range of coherence values, lacking only population in the tiny clusters (very small coherence) or extremely large coherence range. Here, the marginal coherence distributions, integrated over either all negative or all positive energies, are strikingly different (not shown here).

The bottom two panels show the results for a two-dimensional gas. For both anisotropic and isotropic interactions the overall coherence lengths are smaller than in three-dimensions, but still exhibit large peaks near zero energy. The isotropic distribution still shows a sharp asymmetry, with a wide spread of delocalized states at positive energies. One notable difference can be seen in the highest probability peaks of both distributions (red color), which are prominent at blue detuning for the anisotropic interaction but at red detuning for the isotropic interaction. This sign change is related with the fact that the anisotropic case has both positive and negative interactions, while in the isotropic case where it is purely non-negative.

### 3.1. Role of interactions in delocalization

The nature and properties of these delocalized states – their asymmetry with respect to positive and negative energies, their differences in two and three dimensions, their large sizes – are necessarily linked rather subtly to the matrix elements in the Hamiltonian. In this section we examine three different modifications to these matrix elements and therefore to test the stability of these states and to reveal aspects of their structure.

Static energy fluctuations and decoherent processes are known to lead to localization in many systems. A sophisticated study of these effects requires a full inclusion of this physics into the evolution of the density matrix, which is beyond the scope of this article. However, we can perform a proof of principle test of the robustness of these delocalized states by

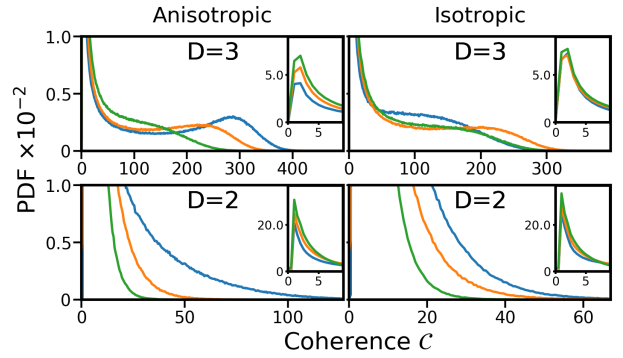


**Figure 4.** Coherence distributions for the  $\alpha = 3$  interaction and four different cutoff values  $W$ : 0 (blue), 0.05 (orange), 0.1 (green), all in units of  $E_{\text{ref}}(D)$ . The coherence binwidth is 1. The insets show a closeup of the small coherence region.

modifying the Hamiltonian to include diagonal disorder, i.e. by adding uniformly distributed  $\varepsilon_n$  to the on-site energies  $\varepsilon_n$ . As seen in Fig. 3, even at disorder strengths  $V$  on the order of the energy unit  $E_{\text{ref}}(D)$  we do not observe any significant changes in the distributions. In the insets we see that the decoupled strongly-interacting cluster distribution is completely unaffected by this disorder.

As a second check of robustness, we apply a cutoff to the interactions between atoms, setting all matrix elements smaller than a given value  $W$  to zero. Although this specific model does not correspond to a specific physical mechanism, it tests if the stability of these delocalized states is contingent on very fragile long-range networks bound by weak interactions. As shown in Fig. 4, we see that the delocalized states are robust against the removal of even quite large

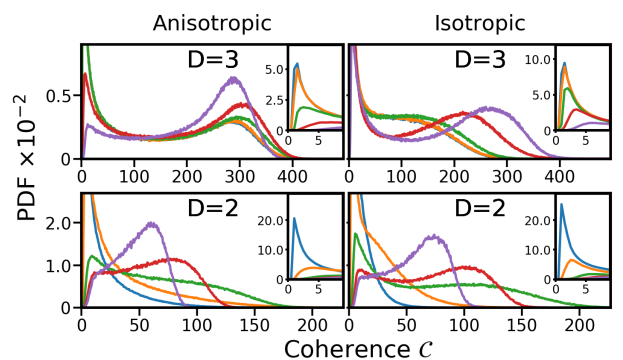


**Figure 5.** Coherence distributions for the  $\alpha = 3$  interaction and five different blockade radii ( $R_B$ ): 0 (blue), 0.25 (orange), 0.5 (green), and 0.75 (red), and 1.0 (purple), all in units of  $a_{\text{ref}}(D)$ . The coherence binwidth is 0.5. To compare similar energy scales between two and three-dimensional systems, since the blockade radius is the same in both cases, we changed the density of the two-dimensional system so that  $E_{\text{ref}}(D = 2) = E_{\text{ref}}(D = 3)$ .

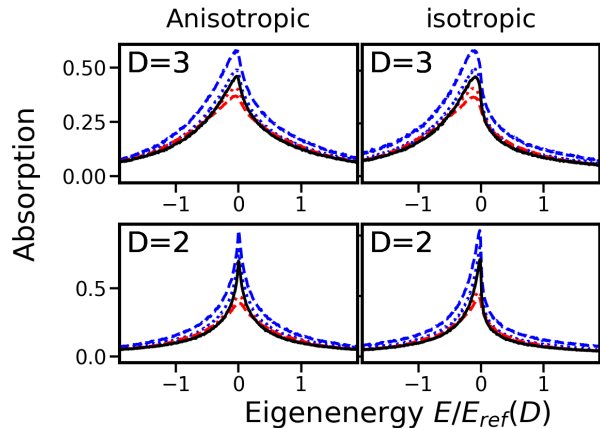


**Figure 6.** Absorption as a function of blockade radius and disorder. The black curve gives the result with  $R_B = 0$  and no disorder; red curves have  $R_B = 0$  and disorder added with  $V = 0.5 E_{\text{ref}}(D)$  (dotted) or  $V = 1 E_{\text{ref}}(D)$  (dashed). The blue curves have no disorder and  $R_B = 0.5 a_{\text{ref}}(D)$  (dotted) or  $R_B = 0.75 a_{\text{ref}}(D)$  (dashed).

interactions, further confirming their stability and also demonstrating that these states are based on extended networks of strongly interacting atoms. We observe that the number of very small clusters increases with increasing cutoff strength, as evinced by the insets. One curious note is that the delocalized states are more stable against this loss in the isotropic case than in the anisotropic, and indeed in three-dimensions the largest coherence lengths even grow when these interactions are clipped.

The final interaction modification is the removal of large interactions in the gas, which can be realized experimentally via the Rydberg blockade. By imposing the blockade at various strengths we prevent the formation of small clusters of strongly interacting atoms on the scale of  $R_B$ , and hence remove the high-energy tails of the distributions. As seen in the distributions in Fig. 5 the increasing Rydberg blockade radius manifests itself in a shifting of population from highly localized states into delocalized arrangements. Eventually, and particularly in the two-dimensional system, the Rydberg blockade eliminates all small clusters, as previously seen in Ref. [28].

As expected from these results, the eigenvalue distribution (not shown here) and the absorption spectrum, shown in Fig. 6, are nearly unaffected by the disorder or by the Rydberg blockade in the energy range around zero. However, these distributions also reveal very little of the structure seen in the coherence distributions of Fig. 2, in particular the large asymmetries and very noticeable distinctions between different dimensions and anisotropies. This is seen in the solid black curves in all panels, and reflects the

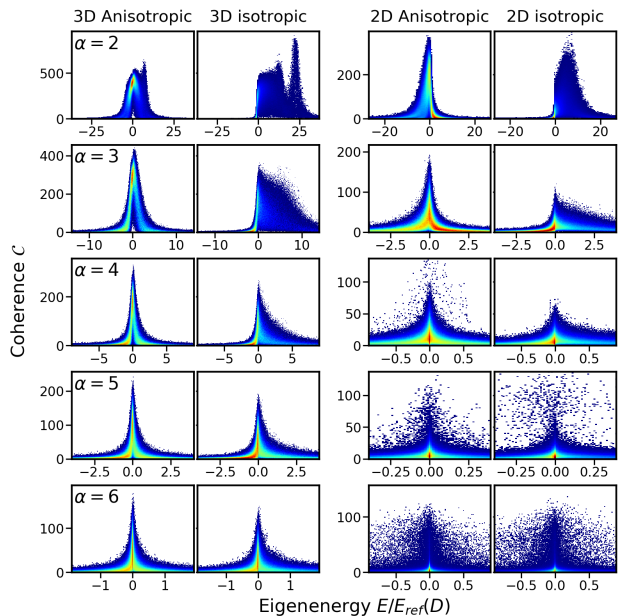


**Figure 7.** Distribution of coherence and eigenenergies for various power-law interactions, in 2D and 3D and with/without anisotropy. The coherence binwidth is 1 and energy binwidth is 0.01.

observation that large delocalization does not imply large absorption.

#### 4. Power law dependence

It is instructive to consider also other power law exponents to study the role of the interaction strength and effective range on the delocalization and to better understand the behaviour of the  $\alpha = 3$  power law. We calculate eigenstates for a variety of power laws,  $\alpha = 2, 3, \dots, 6$ , to obtain the coherence and eigenenergy distributions shown in Fig. 7. Clearly, the coherence lengths and amount of asymmetry increase with the range of the interaction. This asymmetry continues to be strongest in the isotropic case, and particularly for the  $\alpha = 2$  results is manifested by a nearly instantaneous transition from totally localized dimer states as  $E \rightarrow 0^-$  to potentially highly delocalized states as  $E \rightarrow 0^+$ . This observation, borne out of the coherence distribution shown here, is supported by a close inspection of many wave functions for many realizations. We observe an unusual peak structure in the 3D  $\alpha = 2$  results, which is even more dominant in the  $\alpha = 1$  case (not shown). While these power-laws seem to be difficult to realize in a Rydberg setup, they might be relevant in other randomly arranged nanosystems.

## 5. Conclusions

Through our study of the eigenstates of an interacting random Rydberg gas, we have seen that the surprisingly high amount of delocalization in these states observed in Ref. [28] persists in both 3D and 2D gases. These delocalized states are very robust against a range of disorder or decoherence processes. The Rydberg blockade, by creating a more regular arrangement array of background  $\downarrow$  atoms, leads to even larger degrees of delocalization. These delocalized states persist for the various power-law interactions studied here.

To observe these states, it is clearly insufficient to simply measure the absorption spectrum of the gas as shown in Fig. 6. As demonstrated in Ref. [28], one can use strong microwave pulses of well-determined durations and Rabi frequencies to selectively populate delocalized states and probe them directly. The existence of such delocalized states has implications for non-linear spectroscopy of many-body states in randomly arranged systems since the localization of many-body states will be determined by the extent of the underlying one-exciton domains.

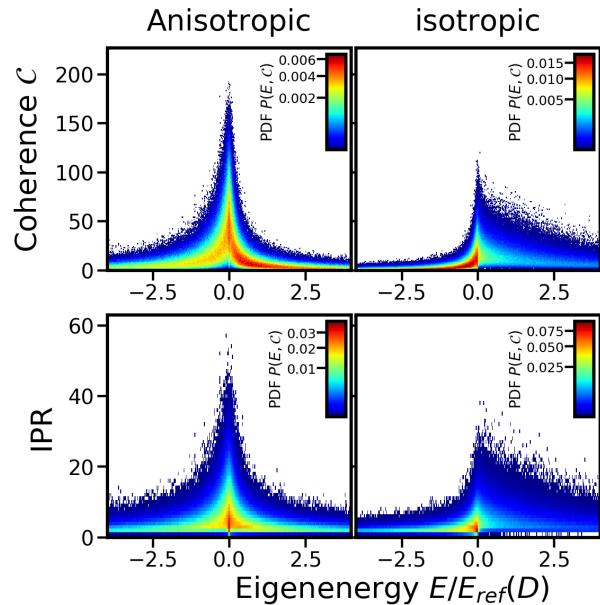
## Acknowledgments

We acknowledge funding from the DFG: grant EI 872/4-1 through the Priority Programme SPP 1929 (GiRyd). AE acknowledges support from the DFG via a Heisenberg fellowship (Grant No EI 872/5-1). MTE acknowledges support from an Alexander von Humboldt Stiftung postdoctoral fellowship.

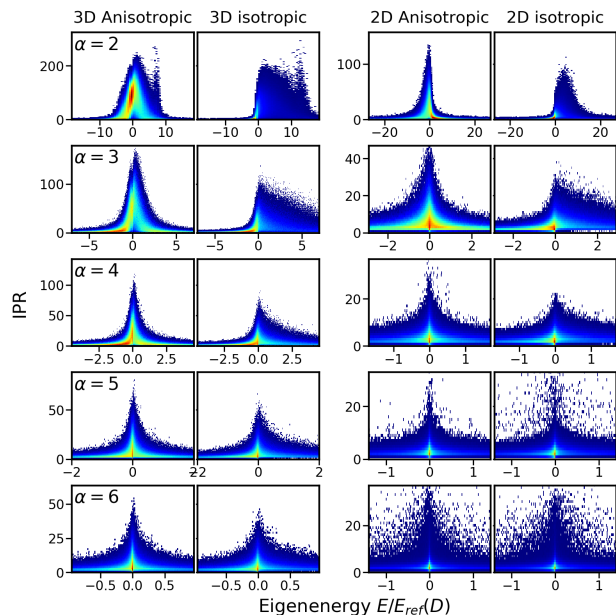
## Appendix I: Comparison of coherence and inverse participation ratio

Fig. 8 compares the distributions of coherence values with the distributions of IPRs for the two-dimensional gas. The distributions are rather similar in overall shape and structure except for an overall scale factor. However, closer inspection reveals that the IPR does not exhibit the strong asymmetry in the localized states close to zero eigenenergy that is so evident in the coherence; this furthermore limits its utility in differentiating the isotropic and anisotropic coherence distributions.

This is true for all power law interactions, as seen in Fig. 9, although in the 3D case the distribution is still markedly asymmetric. For this reason, although for most features the IPR and coherence provide equivalent information about delocalization, coherence is a slightly more sensitive measure especially in two dimensions.



**Figure 8.** Distribution of coherence values and eigenenergies (top) and IPR and eigenenergies (bottom) for the two-dimensional gas. The coherence and IPR binwidth is 0.5 and the energy binwidth is 0.01.



**Figure 9.** IPR and energy distributions for the the various power-law interactions. The IPR binwidth is 0.5 and the energy binwidth is 0.01.

## References

- [1] Saikin S K, Eisfeld A, Valleau S and Aspuru-Guzik A 2013 *Nanophotonics* **2** 21
- [2] van Amerongen H, Valkunas L and van Grondelle R 2000 *Photosynthetic Excitons* (World Scientific, Singapore)
- [3] Yan B, Moses S A, Gadway B, Covey J P, Hazzard K R,

- Rey A M, Jin D S and Ye J 2013 *Nature* **501** 521
- [4] Barredo D, Labuhn H, Ravets S, Lahaye T, Browaeys A and Adams C S 2015 *Phys. Rev. Lett.* **114** 113002
- [5] Dai X, Richter M, Li H, Bristow A D, Falvo C, Mukamel S and Cundiff S T 2012 *Phys. Rev. Lett.* **108**(19) 193201
- [6] Bruder L, Binz M and Stienkemeier F 2015 *Phys. Rev. A* **92** 053412
- [7] Bruder L, Eisfeld A, Bangert U, Binz M, Jakob M, Uhl D, Schulz-Weiling M, Grant E R and Stienkemeier F 2019 *Phys. Chem. Chem. Phys.* 2276–2282
- [8] Feng G, Cundiff S T and Hebin L 2016 *Opt. Lett.* **41** 2954–2957
- [9] Yu S, Titze M, Zhu Y, Liu X and Li H 2019 *Optics Express* **27** 28891–28901
- [10] Mukamel S 2016 *The Journal of Chemical Physics* **145** 041102
- [11] Li Z Z, Bruder L, Stienkemeier F and Eisfeld A 2017 *Phys. Rev. A* **95** 052509
- [12] Mourachko I, Comparat D, de Tomasi F, Fioretti A, Nosbaum P, Akulin V M and Pillet P 1998 *Phys. Rev. Lett.* **80**(2) 253–256
- [13] Anderson W R, Veale J R and Gallagher T F 1998 *Phys. Rev. Lett.* **80**(2) 249–252
- [14] Mourachko I, Li W and Gallagher T F 2004 *Phys. Rev. A* **70**(3) 031401
- [15] Scholak T, Wellens T and Buchleitner A 2014 *Physical Review A* **90** 063415
- [16] Pillet P, Comparat D, Muldrich M, Vogt T, Zahzam N, Akulin V M, Gallagher T F, Li W, Tanner P, Noel M W and Mourachko I 2005 Coherence and decoherence in rydberg gases *Decoherence, Entanglement and Information Protection in Complex Quantum Systems* (Springer-Verlag) pp 411–436
- [17] Singer K, Stanojevic J, Weidemüller M and Côté R 2005 *Journal of Physics B: Atomic, Molecular and Optical Physics* **38** S295–S307
- [18] Weber S, Tresp C, Menke H, Urvoy A, Firstenberg O, Büchler H P and Hofferberth S 2017 *Journal of Physics B: Atomic, Molecular and Optical Physics* **50** 133001
- [19] Afrousheh K, Bohlouli-Zanjani P, Vagale D, Mugford A, Fedorov M and Martin J D D 2004 *Phys. Rev. Lett.* **93**(23) 233001
- [20] Park H, Tanner P J, Claessens B J, Shuman E S and Gallagher T F 2011 *Physical Review A* **84**
- [21] Löw R, Weimer H, Nipper J, Balewski J B, Butscher B, Büchler H P and Pfau T 2012 *Journal of Physics B: Atomic, Molecular and Optical Physics* **45** 113001
- [22] Saffman M 2016 *Journal of Physics B: At. Mol. Opt. Phys.* **49** 202001
- [23] Saffman M, Walker T G and Mölmer K 2010 *Rev. Mod. Phys.* **82** 2313
- [24] Raimond J, Vitrant G and Haroche S 1981 *Journal of Physics B: Atomic and Molecular Physics* **14** L655
- [25] Vogt T, Viteau M, Zhao J, Chotia A, Comparat D and Pillet P 2006 *Phys. Rev. Lett.* **97**(8) 083003
- [26] Ravets S, Labuhn H, Barredo D, Lahaye T and Browaeys A 2015 *Phys. Rev. A* **92**(2) 020701
- [27] Robicheaux F, Hernández J V, Topçu T and Noordam L D 2004 *Physical Review A* **70**
- [28] Abumwis G, Eiles M T and Eisfeld A 2019 *arXiv:1909.12705*
- [29] Chomaz L, Corman L, Bienaimé T, Desbuquois R, Weitenberg C, Nascimbène S, Beugnon J and Dalibard J 2015 *Nature communications* **6** 6162
- [30] Müller M, Paulheim A, Eisfeld A and Sokolowski M 2013 *J. Chem. Phys.* **139** 044302
- [31] Müller M, Paulheim A, Marquardt C and Sokolowski M 2013 *J. Chem. Phys.* **138** 064703
- [32] Park H, Tanner P J, Claessens B J, Shuman E S and Gallagher T F 2011 *Phys. Rev. A* **84** 022704
- [33] Baumgratz T, Cramer M and Plenio M B 2014 *Phys. Rev. Lett.* **113**(14) 140401
- [34] Lukin M D, Fleischhauer M, Cote R, Duan L M, Jaksch D, Cirac J I and Zoller P 2001 *Physical Review Letters* **87**
- [35] Tong D, Farooqi S, Stanojevic J, Krishnan S, Zhang Y, Côté R, Eyler E and Gould P 2004 *Physical Review Letters* **93** 063001
- [36] Gaëtan A, Miroshnychenko Y, Wilk T, Chotia A, Viteau M, Comparat D, Pillet P, Browaeys A and Grangier P 2009 *Nature Physics* **5** 115
- [37] Urban E, Johnson T A, Henage T, Isenhower L, Yavuz D, Walker T and Saffman M 2009 *Nature Physics* **5** 110
- [38] Ates C, Pohl T, Pattard T and Rost J M 2007 *Physical review letters* **98** 023002
- [39] Pohl T, Demler E and Lukin M D 2010 *Physical review letters* **104** 043002
- [40] Schauß P, Cheneau M, Endres M, Fukuhara T, Hild S, Omran A, Pohl T, Gross C, Kuhr S and Bloch I 2012 *Nature* **491** 87
- [41] Li W, Tanner J P, Jamil Y and Gallagher T F 2006 *Eur. Phys. J. D* **40** 27–35
- [42] Li W, Tanner P J, Jamil Y and Gallagher T F 2006 *The European Physical Journal D* **40** 27–35
- [43] Li W, Noel M W, Robinson M P, Tanner P J, Gallagher T F, Comparat D, Laburthe Tolra B, Vanhaecke N, Vogt T, Zahzam N, Pillet P and Tate D A 2004 *Phys. Rev. A* **70**(4) 042713
- [44] Li W, Tanner P J and Gallagher T F 2005 *Phys. Rev. Lett.* **94**(17) 173001
- [45] Ates C, Eisfeld A and Rost J M 2008 *New J. Phys.* **10** 045030
- [46] Wüster S, Eisfeld A and Rost J M 2011 *Phys. Rev. Lett.* **106** 153002